UNIVERSITY OF LEEDS

This is a repository copy of *Heteroprotein complex formation of bovine lactoferrin and pea protein isolate: A multiscale structural analysis*.

White Rose Research Online URL for this paper:
http://eprints.whiterose.ac.uk/110783/

Version: Accepted Version

Article:
Adal, E, Sadeghpour, A, Connell, S orcid.org/0000-0003-2500-5724 et al. (3 more authors) (2017) Heteroprotein complex formation of bovine lactoferrin and pea protein isolate: A multiscale structural analysis. Biomacromolecules, 18 (2). pp. 625-635. ISSN 1525-7797

https://doi.org/10.1021/acs.biomac.6b01857

© 2017, American Chemical Society. This document is the Accepted Manuscript version of a Published Work that appeared in final form in Biomacromolecules, copyright © American Chemical Society after peer review and technical editing by the publisher. To access the final edited and published work see https://doi.org/10.1021/acs.biomac.6b01857.

Reuse
Unless indicated otherwise, fulltext items are protected by copyright with all rights reserved. The copyright exception in section 29 of the Copyright, Designs and Patents Act 1988 allows the making of a single copy solely for the purpose of non-commercial research or private study within the limits of fair dealing. The publisher or other rights-holder may allow further reproduction and re-use of this version - refer to the White Rose Research Online record for this item. Where records identify the publisher as the copyright holder, users can verify any specific terms of use on the publisher's website.

Takedown
If you consider content in White Rose Research Online to be in breach of UK law, please notify us by emailing eprints@whiterose.ac.uk including the URL of the record and the reason for the withdrawal request.

White Rose university consortium
Universities of Leeds, Sheffield & York

eprints@whiterose.ac.uk
https://eprints.whiterose.ac.uk/

Heteroprotein complex formation of bovine lactoferrin and pea protein isolate: A multiscale structural analysis

Eda Adal[1,2], Amin Sadeghpour[1], Simon Connell[3], Michael Rappolt[1], Esra Ibanoglu[2], Anwesha Sarkar[1]*.

[1]*Food Colloids and Processing Group, School of Food Science and Nutrition, University of Leeds, Leeds, LS2 9JT, United Kingdom,*

[2]*Gaziantep University, Food Engineering Department, 27310 Gaziantep, Turkey*

[3]*Molecular and Nanoscale Physics Group, School of Physics and Astronomy, University of Leeds, Leeds, LS2 9JT, United Kingdom.*

KEYWORDS. Lactoferrin, pea protein, complex coacervation, small angle X-ray scattering (SAXS), atomic force microscopy (AFM).

ABSTRACT

Associative electrostatic interactions between two oppositely charged globular proteins, lactoferrin (LF) and pea protein isolate (PPI), the latter being a mixture of vicilin, legumin and convicilin, was studied with a specific PPI/ LF molar ratio at room temperature. Structural aspects of the electrostatic complexes probed at different length scales were investigated as a function of pH by means of different complementary techniques, namely with dynamic light scattering, small angle X-ray scattering (SAXS), turbidity measurements and atomic force microscopy (AFM). Irrespective of the applied techniques, the results consistently displayed that complexation between LF and PPI did occur. In an optimum narrow range of pH 5.0-5.8, a viscous liquid phase of complex coacervate was obtained upon mild centrifugation of the turbid LF-PPI mixture with a maximum R_h, turbidity and the ζ-potential being close to zero observed at pH 5.4. In particular, the SAXS data demonstrated that the coacervates were densely assembled with a roughly spherical size distribution exhibiting a maximum extension of ~ 80 nm at pH 5.4. Equally, AFM image analysis showed size distributions containing most frequent cluster sizes around 40-80 nm with spherical to elliptical shapes (axis aspect ratio ≤ 2) as well as less frequent elongated to chain-like structures. The most frequently observed compact complexes, we identify as mainly leading to LF-PPI coacervation, whereas for the less frequent chain-like aggregates, we hypothesize that additionally PPI-PPI facilitated complex existed.

1. INTRODUCTION

Interaction of oppositely charged biopolymers in aqueous media, mostly driven by electrostatic forces can lead to a spontaneous liquid-liquid phase separation into biopolymer-rich phase (coacervate phase) and solvent-rich phase [1]. During initial stages, the biopolymer molecules tend to form intrapolymeric soluble complexes. Further electrostatic interaction leads to the formation of a dense and viscous liquid phase (coacervate) from a homogeneous macromolecular solution of poor solvency as a result of thermodynamic incompatibility. The significance of complex coacervation ranges from its natural occurrence in biological systems, such as providing the outer physical protection of mussels and sand castle worms [2], to biomedical applications, such as scaffold based tissue engineering [3], drug delivery [4] and various food applications, such as biodegradable films, fat replacer and meat analogues [5]. Type and size of biopolymers, mixing ratio, total biopolymer concentration, chain conformation and flexibility, distribution of reactive groups and the charge density, solvent conditions (pH, ionic strength and temperature), stirring and pressure are important physicochemical parameters influencing the associative interaction between the two biopolymers [6].

Although complex coacervation has been studied in a wide range of polyelectrolyte systems, protein-protein complex coacervation is a relatively new undertaking. Understanding the mechanism of the heteroprotein complex coacervation will open enormous opportunities for immediate use in food and non-food applications (pharmaceuticals, cosmetics, biomedicals), where biocompatibility is a key issue. Heteroprotein complex coacervation between cationic lactoferrin (LF) and anionic β-lactoglobulin [7-13] as well as casein [14, 15] has captured much research attention in recent years. Yan and co-workers [9] observed that LF and BLG coacervates were formed at very low salt concentration and narrow pH range around 5.7−6.2, which has been

recently confirmed by Peixoto and coworkers [12] using fluorescence intensity measurements and nuclear magnetic resonance. On the other hand, Anema and de Kruif [16] observed that the coacervation of lactotransferrin and β-lactoglobulin over a relatively wide pH range of pH 5-7.3 and higher ionic strength. Studies by Nigen et al. showed presence of both coacervation and complexation with presence of unique micro-spherical particles between lysozyme and calcium-depleted α-lactalbumin (apo α-LA) [17], both processes being largely temperature dependent [18].

In this study, we utilized two globular proteins: lactoferrin (LF) and a mixed plant protein, pea protein isolate (PPI). Lactoferrin (LF) is a metal-binding glycoprotein with a molar mass of 80 kDa and a high isoelectric point (pI) of ~8.5 providing it a novel feature of maintaining positive charge over a wide range of pH [9]. Pea (Pisum sativum L.) is an important vegetable source of protein and has attracted significant research attention because of its biological value, functional properties in food applications, and relatively low cost. Pea protein is dominated by two major globulin (legumin and vicilin) and one minor (convicilin) proteins. Pea protein is limited in sulphur-containing amino acids, so it might be a strategy to complement the protein with dairy protein, the latter being rich in all essential amino acids. To our knowledge, there are no reported studies on heteroprotein coacervation between LF and plant protein. Nonetheless, LF/ PPI coacervate-based biomaterials can not only lead to a novel class of food matter, but can potentially be employed in a wide range of applications. However, to design such a functional coacervate, efforts must be undertaken to identify the precise range of working conditions for formation of complexes, coacervate and their structural aspects at different length scales.

The objective of this study was to identify the conditions for creation of LF/ PPI heteroprotein coacervate and complexes, which were characterized by electrophoretic mobility, dynamic light scattering (DLS) and turbidimetry. In addition, SAXS (small-angle X-ray scattering) and AFM

(atomic force microscopy) were employed to gain structural insights of the LF-PPI complexes and coacervate at specified conditions.

2. EXPERIMENTAL SECTION

2.1.Materials.

The bovine lactoferrin (LF) was kindly donated by Ingredia Nutritional (Arras, France). According to the technical specification provided by the supplier, it was purified from bovine milk and contained 96% protein, 0.5% ash and iron saturation was 10-20%. Pea protein isolate (PPI) (Nutralys®) was obtained from Roquette (Lestrem, France) and contained 85% protein, 7% moisture, and 4% ash. Sodium azide was purchased from Sigma-Aldrich Chemical Company (St. Louis, MO, USA). Milli-Q water (water purified of 18.2 M Ω.cm by Milli-Q apparatus, Millipore Corp., Bedford, MA, USA) was used as a solvent in all experiments. Hydrochloric acid (1 N HCl) and sodium hydroxide (1 N NaOH) were diluted from concentrated ~37% w/v) HCl-water solution or 10 M NaOH solution (Sigma-Aldrich), respectively.

2.2.LF-PPI Complex and Coacervate Preparation.

Dispersions of LF (4 g/L) and PPI (4g/L) were prepared by dissolving an exact amount of LF powder or PPI powder in Milli-Q water, respectively for 2 h at 25 °C using a magnetic stirrer to ensure complete solubilisation. The dispersions were centrifuged at 20,000 × g for 30 minutes, filtered through Whatman No. 4 filter paper and 0.22 µm syringe filter to remove any residues. The resultant LF stock solution showed 99.8% soluble protein yield, whereas PPI showed 30% soluble protein yield, i.e. referring to a concentration of 1.2 g/L measured by using Kjeldahl analysis (AOAC 981.10) [19]. Note that this soluble fraction of PPI is further on referred to as the PPI stock solution. The mineral composition analysed using ICP-MS (Inductively Coupled Plasma

Mass Spectrometry) of the stock solutions was the following (g/100 g): LF: Na 0.0568, K 0.0017, Mg < detection limit (0.00004), Ca 0.0022, Fe 0.025, P 0.050 and PPI: Na 0.2542, K 0.0588, Mg 0.0086, Ca 0.0077, Fe 0.00043, P 0.1637. Different semi-dilute concentrations of PPI working solutions (0.00035-0.07 mM) were prepared by dilution of the PPI stock solution (1.2 g/L, i.e. 0.07 mM) using Milli-Q water. Appropriate volumes of PPI and LF at pH 7.0 were mixed for the molar ratio study. The molar concentrations of LF and PPI were calculated using respective molecular weights (discussed in SDS-PAGE section) and the molar ratio was based on the assumption that all different fractions of PPI (legumin, vicilin, convicilin) participated equally in complex formation with LF in the same ratio as they existed in the working solutions. For the pH study, the pH of PPI/ LF with a molar ratio of 0.15 (mixture of 0.007 mM PPI and 0.047 mM LF) was adjusted to target pH from pH 2-9 using 1 N standard HCl or NaOH as shown in Figure 1 magnetic stirring conditions (500 rpm). Appropriate volumes (5.0 mL) of LF stock solution was rapidly poured into an equal volume of freshly prepared PPI working solutions in a beaker followed by mixing at 500 rpm. As described in previous literature [9], for "high to low", PPI and LF working solutions at pH 9.0 were mixed and then the mixtures were rapidly adjusted to a target pH while mixing. For "low to high", LF and PPI solutions were mixed at pH 2.0 and then the mixtures were adjusted to a target pH quickly while mixing. The polymer-rich phase (coacervate) was collected using mild centrifugation at 500 × g for 10 minutes and characterized using AFM, SAXS and TEM. Sodium azide (0.02 wt%) was added to prevent any bacterial growth in samples only at ≥ pH 7.0. No significant difference in coacervate structure were observed in terms of sizing, turbidity measurements and zeta potential as compared to fresh samples without the addition of 0.02 wt% azide in above-mentioned pH conditions.

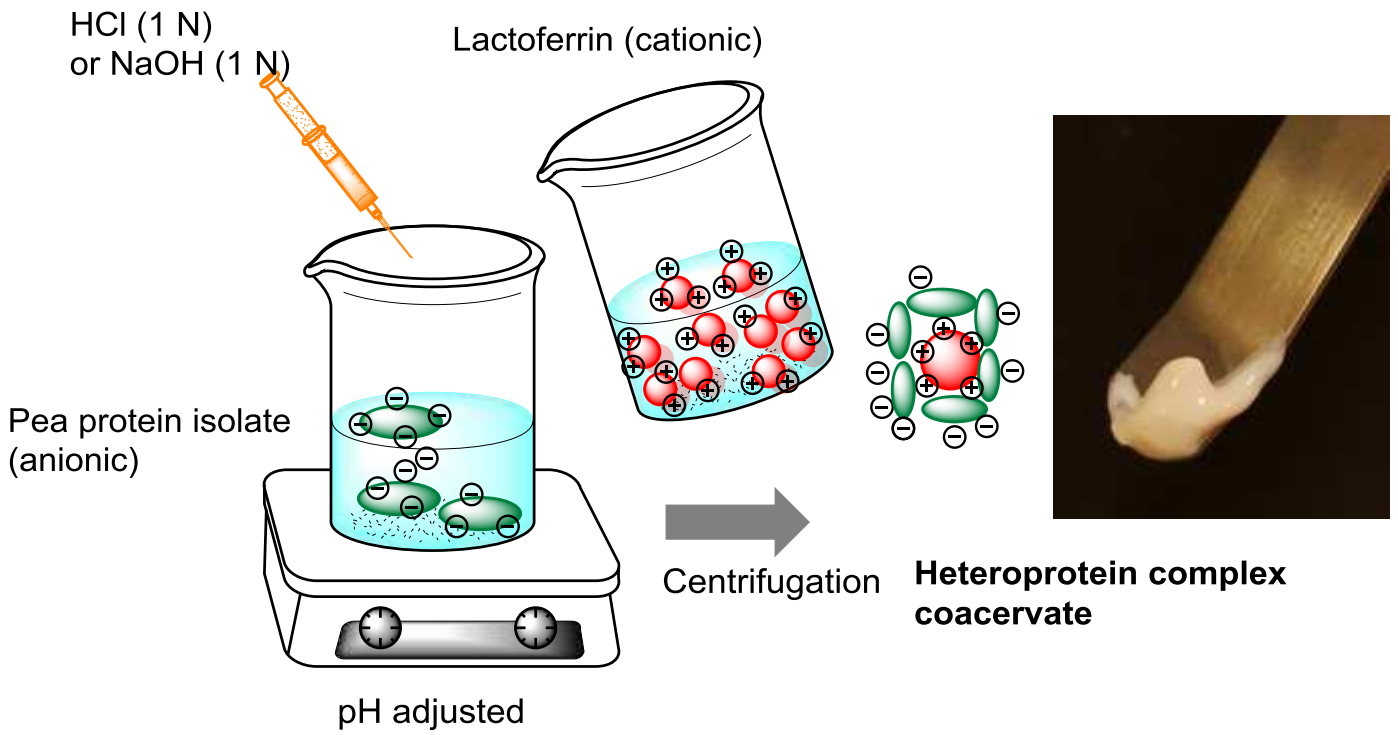

Figure 1. Schematic illustrations of steps of production of heteroprotein complex coacervate showing the visual aspect of the viscous phase (macroscale).

2.3. Size and ζ-potential Measurements.

The mean hydrodynamic radius (R_h) of the pure protein solutions, complex and coacervate was measured by dynamic light scattering (DLS) at 25 °C equipped with a 4 mW helium/neon laser at a wavelength output of 633 nm. Sizing was performed at 10 s intervals in disposable plastic cuvettes (ZEN 0040) using noninvasive backscattering at a detection angle of 173 °C. Assuming the scattering particles to be spherical, their apparent hydrodynamic radius was calculated from the diffusion parameters using Stokes-Einstein equation, i.e. $R_h = k_B T/(6\pi\eta DT)$, where k_B is the Boltzmann constant, T is absolute temperature, and η is solvent viscosity.

The ζ-potential values of the pure protein solutions, their complexes and coacervates were measured using a laser Doppler velocimetry and phase analysis light scattering (M3-PALS0) using disposable electrophoretic mobility cells (DTS 1060). The effective electric field, E, applied in the

144 measurement cell was between 50 and 150 V. The electrophoretic mobility, μ, was calculated
145 assuming spherical particles at 20 °C according using Equation 1:

146 $$\mu = \frac{v}{E} \quad (1)$$

147 where, v is the drift velocity of a dispersed particle (m/s) and E is the applied electric field strength.
148 The ζ-potential (mV) was calculated via the Smoluchowski Equation 2:

149 $$\mu = \frac{\xi\varepsilon}{\eta} \quad (2)$$

150 which is valid for $r >> \kappa^{-1}$, where ε is the electric permittivity of the solvent, η is the solvent
151 viscosity (Pa s), r is the radius of particle and κ^{-1} is the Debye length. Both Z-average diameter and
152 ζ-potential were measured with a Zetasizer Nano ZS (Malvern Instruments Ltd, Malvern,
153 Worcestershire, UK). The results were reported as mean Z-average mean diameter or mean ζ-
154 potential of five readings and standard deviations were calculated.
155

156 **2.4. Turbidity Measurements**

157 The turbidity of pure protein solutions and their complex/ coacervate were measured by a Jenway
158 6715 UV-Visible Spectrophotometer (Bibby Scientific Limited, Beacon Road, Stone,
159 Staffordshire, ST15 OSA, UK) using 1 cm disposable plastic cuvette at 600 nm. Milli-Q water was
160 used as blank reference resulting in 100% transmittance. The turbidity (T) was calculated using
161 equation (3):

162 $$T = -\ln\frac{I}{I_0} \quad (3)$$

163 where, I is the transmitted intensity and I_0 is the incident light intensity.
164

2.5. Small-angle X-ray scattering (SAXS).

Small angle X-ray scattering (SAXS) patterns were recorded in order to determine the size (radius of gyration) of 0.007 mM PPI stock solution, 0.047 mM LF at pH 7.0 and their complexes or coacervates at pH 5.4, 5.8, 6.2 and 7.0, respectively. The SAXS camera set-up (SAXSpace, Anton Paar, Austria) is described in great detail elsewhere [20]. Briefly, the collimation block unit vertically focuses a line shaped beam of Cu-K_α radiation with a wavelength, $\lambda = 0.154$ nm on to the detector plane. For the SAXS experiments the high resolution mode was chosen, which permits to detect a minimum scattering vector, q_{min}, of 0.04 nm^{-1} ($q = (4\pi/\lambda) \sin\theta$, where 2θ is the scattering angle). All studied samples were filled into the same vacuum-tight, reusable 1 mm quartz capillary to guarantee exactly the same scattering volume. The capillary was placed in the temperature controlled sample stage at 25 °C ± 0.1 °C. All samples as well as the aqueous buffers and empty capillaries were exposed for 120 minutes. The SAXStreat software (Anton Paar) was used to correct the scattering patterns with respect to the position of the primary beam. The SAXS data was further transmission-corrected by setting the attenuated scattering intensity at q = 0 to unity and the background was subtracted using the SAXS Quant software (Anton Paar). The scattering vector q was calibrated with silver-behenate, which has a known lattice spacing of 5.84 nm. The reduced scattering pattern were finally analyzed with the GIFT software package in order to fit the scattering data by Indirect Fourier Transformation (IFT), generate the Pair-Distance Distribution Functions (PDDF) and to determine the radius of gyration of the pure proteins and their coacervates.

2.6.Atomic force microscopy (AFM) Measurements.

Complexes, coacervate and pure proteins were investigated with an Icon Fast-Scan Bio Atomic Force Microscope (Bruker Nano Surfaces, Santa Barbara, CA). Samples were prepared for deposition by serial dilution of the stock solutions at the required pH. Good dispersions were generally found at a dilution of 1×10^6 times, and continuous films at 100× dilution. 20 μL of each diluted sample was pipetted onto a freshly cleaved ruby mica disc and incubated for 5 minutes, before rinsing with approximately 5 mL of Milli-Q water, drying by wicking onto filter paper followed by a stream of nitrogen. The LF and LF-PPI complex at lower pH value (pH 5.4) adhered well, but the complex at pH 7.0 would only adhere to the mica if it had been pre-treated with Mg^{2+} ions (50 μL of 5 mM $MgCl_2$ solution for half an hour), the rationale being that the charge on the complex was negative hence repelling from the mica which is also negatively charged at neutral pH. Pure PPI did not adhere well to the mica, although lower quality images could be obtained by drying the sample without rinsing. Samples were scanned using TESPA-V2 probes (Bruker) with tapping mode in air, at a resonant frequency of 340-350 kHz and minimum set point, at a typical scan rate of 3-4 Hz depending upon image size. Multiple scans across the samples were obtained to ensure good statistics, typically at 2 μm scan size and 1536 or 2048 pixel resolution. AFM images were analysed using the Particle Analysis function in ImageJ (NIH). Each image was converted into a binary image using a manual threshold to prepare for the automated analysis. The outline of each complex was fitted with an ellipse, with the major and minor axes describing the length and width of each complex respectively. Sizing of the individual proteins was carried out in Nanoscope Analysis software (Bruker, version 1.5) using the manual ruler tool.

2.8 Protein content, solubility curve and composition

Both protein stock solutions (LF and PPI) were examined after centrifugation and filtration for crude protein content (AOAC 981.10). The PPI stock solution (1.2 g/L) was analyzed for its solubility as a function of pH from pH 2-9 [19]. The composition was assessed using sodium dodecyl sulphate polyacrylamide gel electrophoresis (SDS-PAGE) technique. 50 µL of protein solution (at 4 g/L for LF, 1.2 g/L for PPI) was mixed with 50 µL of Laemmli sample buffer (62.5 mM Tris-HCl, 2% SDS 25% glycerol, 0.01% bromophenol blue, 5% β-mercaptoethanol) and the mixture was heated to 95 ° C for 5 min. The samples were cooled to room temperature and 20 µL was loaded onto SDS gels previously prepared on a Mini-PROTEAN II system (Bio-Rad Laboratories). Gels were run for 10 min at 100 mV followed by a phase of 30 minutes at 200 mV. The gels were stained with Coomassie Blue R-250 [0.05% (w/v) in 25.0% (v/v) isopropanol 10.0% (v/v) acetic acid] for at least 4 hours, after which they were destained with water for one hour. Gels were scanned using a flat-bed scanner (Bio-Rad Molecular Imager, Chemi-Dco XRST) and the intensities of the protein bands were quantified using Image LabTM software version 5.1 Beta. The percentage composition of each sample was determined by scanning the areas for each band.

3. RESULTS AND DISCUSSION

Figure 2 shows the SDS-PAGE electrophoretogram of the LF and PPI stock solution tested. Lactoferrin (LF) stock solution (0.047 mM) had protein content of 96% (Kjeldahl, N×6.38), in agreement with the specification stated by the manufacturer of which 95% was lactoferrin (Figure 2). On the other hand, pea protein isolate stock solution (0.007 mM) had protein content of 97% (Kjeldahl, N×6.25) and exhibited a wide variety of polypeptide subunits of molecular weight (M_w) ranging from 20 to 75 kDa, consisting of three main sets of protein subunits i.e. convicillin (72.4-

77.9 kDa, 13.5%), vicillin (28.7-47.3 kDa, 33.2%) and legumin (α-subunits, 40.9 kDa, 21.2%; β-subunit, 22.3-23.1 kDa, 18.1%), which is in agreement with findings of previous authors [21]. The legumin/vicillin (L/V) ratio was 1.2 which is within the lower range of values reported in literature [22]. The solubility curve of PPI stock solution shows that the isoelectric point (pI) is pH 4.0, which is in accordance with previous reports [23].

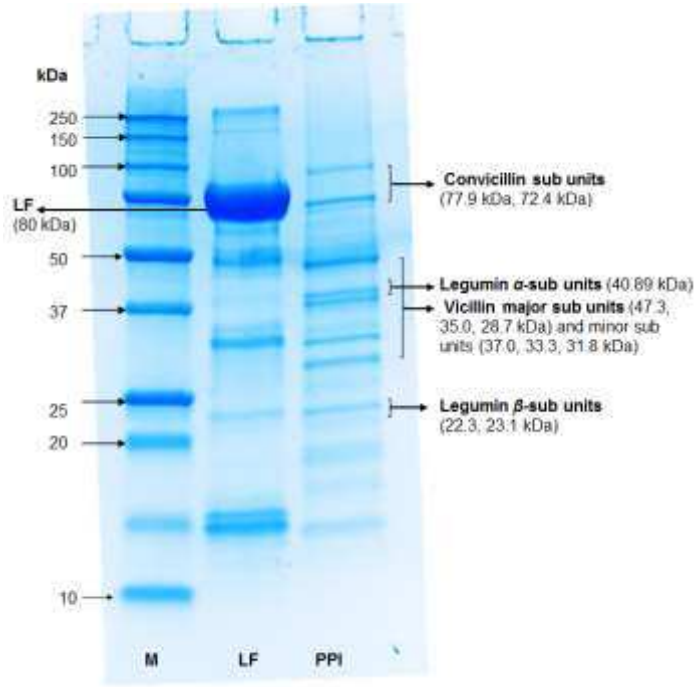

Figure 2. SDS-PAGE of LF (0.047 mM) and PPI (0.007 mM) stock solutions. M is the molecular weight marker (10–250 kDa).

Structure of coacervates formed by proteins with complementary charges are driven by electrostatic interactions. Hence, it is obvious that pH, ionic conditions, molar ratio of the charged moieties, protein characteristics (type, size, shape, molecular weight, and surface charge density) etc. may strongly influence the kinetics and thermodynamics of complex coacervation, and most of these parameters cannot be varied independently of each other [24]. The approach toward charge neutralization can be via alteration of the charge of one or both partner macroions, or alteration of the combining ratio (microstoichiometry) within the complex [25]. In this study, we first discuss the

effect of different molar ratios of PPI/ LF on complex and/or coacervate formation at pH 7. This sets the scene for understanding the effect of the pH on the structure of LF-PPI complexes and coacervates at a fixed PPI/ LF molar ratio and identifies the boundary pH conditions leading to LF-PPI complex coacervation

3.1. Effects of biopolymer mixing ratio on LF-PPI complex formation.

Typically, complexation occurs under solvent conditions, where both biopolymers have opposing charges. Selection of pH 7 was justified for the biopolymer mixing ratio as LF and PPI have a net positive and negative charge, respectively. Figure 3 shows the influence of PPI addition on the hydrodynamic radius and turbidity of the LF as a function of PPI/ LF ratio varying from 0.007 to 0.15 mM at neutral pH. Almost optically clear LF-PPI solutions (Figure 3A) underwent a turbidity onset at > 0.04 mM PPI solution that was measurable with increase of optical density OD_{600} (Figure 3B). The turbidity corresponds to appearance of scattering particles in the medium and the formation of LF-PPI complexes. The OD_{600} exhibited its highest value (0.39) at PPI/LF molar ratio of 0.06, making the solution significantly cloudy indicating the maximum formation of insoluble complexes. Beyond PPI/ LF ratio of 0.06, intermediate levels of turbidity were observed with less cloudy appearance.

To assign the macroscopic turbidity data to hetero-protein coacervation, we used DLS and ζ-potential measurements. As shown in Figure 3B, in agreement with the turbidity data, R_h increased slowly from 51 nm to 57.6 nm as PPI/LF ratio increased by one order of magnitude, followed by maxima (~ 82 nm) at a PPI/ LF ratio of 0.06 and then a decrease. At and above the molar ratio of PPI/ LF of 0.08, the R_h reached a plateau. The effect of biopolymer mixing ratio was critical for controlling the charge balance within the mixed systems.

(A) (B)

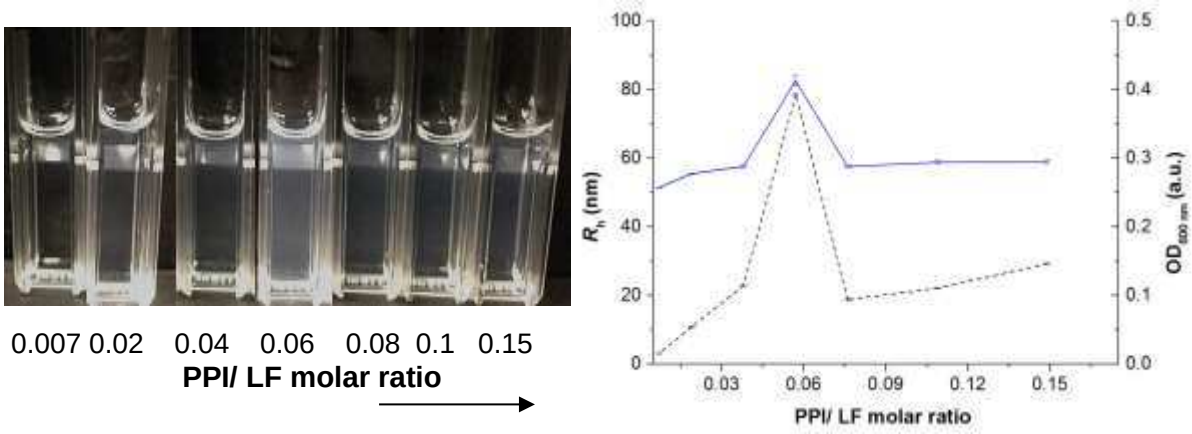

Figure 3. Visual images (A) and dependence of hydrodynamic radius, R_h (bold line), turbidity (dotted line) (B) on PPI/ LF ratio on mixing LF (0.047 mM) with different concentrations of PPI at pH 7. Error bars represent standard deviations. R_h = 8.9 ± 0.13 and 41 ± 0.51 nm and PDI (polydispersity index) equals 0.12 and 0.18 for the pure LF and PPI stock solutions, respectively.

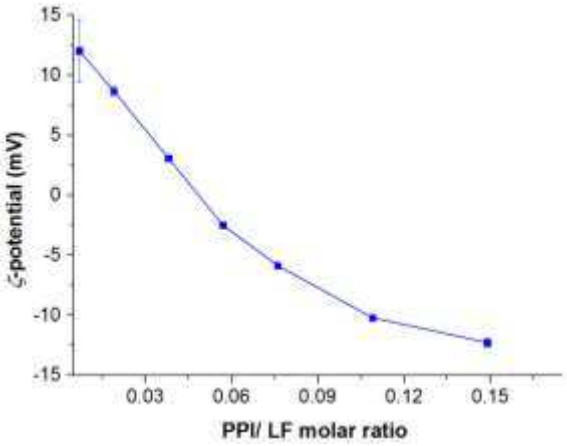

Figure 4. Mean ζ-potential values as a function of PPI/ LF ratio on mixing LF (0.047 mM) with different concentrations of PPI at pH 7. Error bars represent standard deviations.

Zeta potential (ζ), the electro-kinetic potential difference between the dispersion medium and the slip plane (stationary layer of fluid attached to the dispersed particle) of moving particles confirmed an associative driving force for complexation between the positively charged amino acids of LF and the negative charges on PPI at very low biopolymer concentrations (Figure 4). In

283 absence of added PPI, 0.047 mM LF was cationic at pH 7 and the ζ-potential was +12 mV. On
284 addition of PPI, the positive charge of the mixture decreased to be electrically neutral (-2.5 mV)
285 at 0.075 wt%.

286 This means that at molar ratio of PPI/ LF of 0.06, the number of positively charged amino
287 groups were nearly equivalent to that of the carboxylic acid groups, validating charge neutral
288 complex formation, in agreement with the largest R_h and turbidity maxima. Above PPI/LF molar
289 ratio of 0.06, the negative ζ-potential increased steadily to -12.3 mV, which might be attributed to
290 LF molecules being covered by PPI moieties and thus formation of soluble complexes. Similar
291 behavior for mixtures of LF and other proteins showing inter-protein interactions with increase in
292 negative charge of mixed solutions have been observed previously[14]. We selected this PPI/LF ratio
293 of 0.15 to investigate the behavior of rather "soluble LF-PPI complex" with almost no visible
294 turbidity (OD_{600} <0.15) as a function of pH drift in the next section
295

296 **3.2. Effects of pH on coacervate formation.**

297 Hetetoprotein coacervation differs from native protein self-aggregation based on the degree
298 of pH-dependence of complex and kinetics of aggregation[9, 10]. It is known that coacervation
299 can get overshadowed by protein self-aggregation. Hence, the hydrodynamic radius of native
300 LF (0.047 mM), PPI (0.007 mM) and their mixtures at PPI/ LF ratio of 0.15 were measured
301 as a function of pH 2-9 (Figure 5A) to discriminate between self-aggregation (if any) and LF-
302 PPI interaction.

303 There was no significant change in hydrodynamic radius of LF as a function of pH (< 50
304 nm). In the case of PPI, the hydrodynamic radius remained below 80 nm at pH 6 to 9. However,
305 the particle size was higher in the acidic region with possible PPI-PPI self-aggregation reaching

maximum at pH 4 (~ 332 nm), being the isoelectric point of PPI [26]. This trend agrees well with the measured the solubility curve. In the case of LF-PPI mixtures, the hydrodynamic radius remained below 75 nm in all pH except at pH 5-6, where the larger aggregates seemed to appear with maxima at pH 5.4 (Figure 5B). These large sizes might be attributed to the scattering from particles of turbid LF-PPI mixtures. The interaction between LF and PPI did not readily lead to a new "liquid" phase. However, when these turbid materials at pH 5.4 and 5.8 were separated by mild centrifugation, presence of glossy, viscous liquid (Figure 5A, zoomed image in Figure 1) in the Eppendorf tubes had the clear signature of formation of coacervates [14]. As observed in several LF-based coacervate studies [27], the coacervates created might have coalesced into this concentrated viscous phase. The opacity of the viscous phase might suggest the coexistence of pure coacervates and some degree of PPI-PPI linkage facilitated aggregates. Post pH 6.2, the samples were exhibiting rather "one-phase" with 35 nm sized complex.

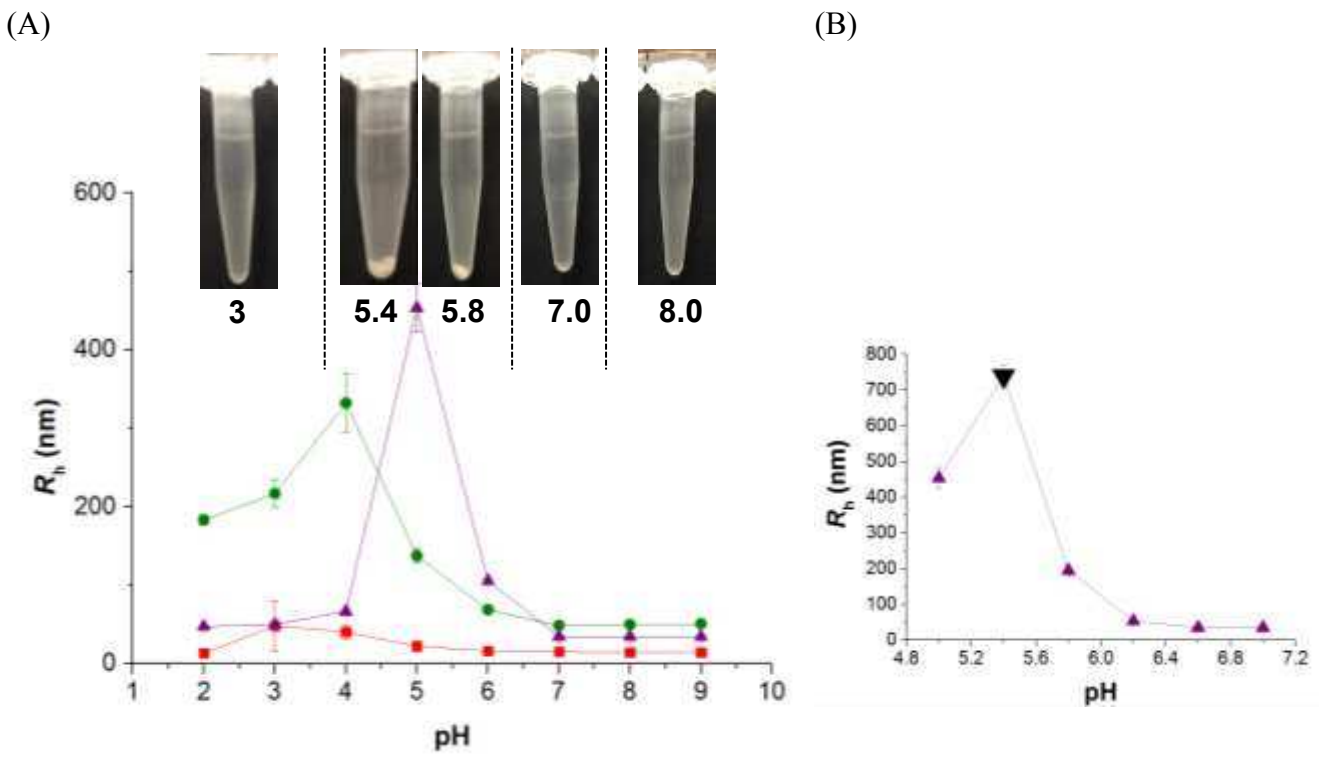

Figure 5. Evolution of hydrodynamic radius, R_h of 0.047 mM LF solution (■), 0.007 mM PPI solution (●) and mixture of 0.047 mM LF and 0.007 mM PPI solutions (▲) (PPI/ LF molar ratio of 0.15) as a function of pH with corresponding visual images taken after mild centrifugation of the LF-PPI mixtures (A) and zoomed-in mean hydrodynamic diameter of LF-PPI mixtures in pH 5-7 region (B). Error bars represent standard deviations.

3.3. Identification of boundary conditions for coacervate formation.

Since complex coacervation between LF and PPI is due to electrostatic interaction between oppositely charged proteins, the charge characteristics of the individual components were measured by Doppler electrophoresis in a wide pH range of 2.0–9.0. (Figure 6). The ζ-potential of LF decreased from +24.8 mV to -1.5 mV as increased pH from 2 to 9 and reached zero at around pH 8.5, which is the isoelectric point of LF. The isoelectric point of LF is in line with the theoretical net charge and fits closely with the pI value reported previously [9].

On the other hand, ζ-potential value of PPI changed from +23.2 mV to -28.2 mV as pH increased and close to zero around pH 4 (pI). This is in line with the increase in R_h data, solubility curve validating the aggregation of pea protein molecules near its isoelectric point. The observed pI of PPI is within the range reported by previous authors [23]. When the LF (0.047 mM) and PPI (0.007 mM) were mixed, the ζ-potential decreased from +32.5 mV to -18.6 mV as a function of pH, with values approximately zero in the pH range from 5-6. Zooming in further the ζ-potential values in pH 5-6, it can be observed that from pH 5-5.8, the ζ-potential values remained ≤ -5 mV and it is only at pH 6.2 and beyond, the negative charge started increasing.

(A) (B)

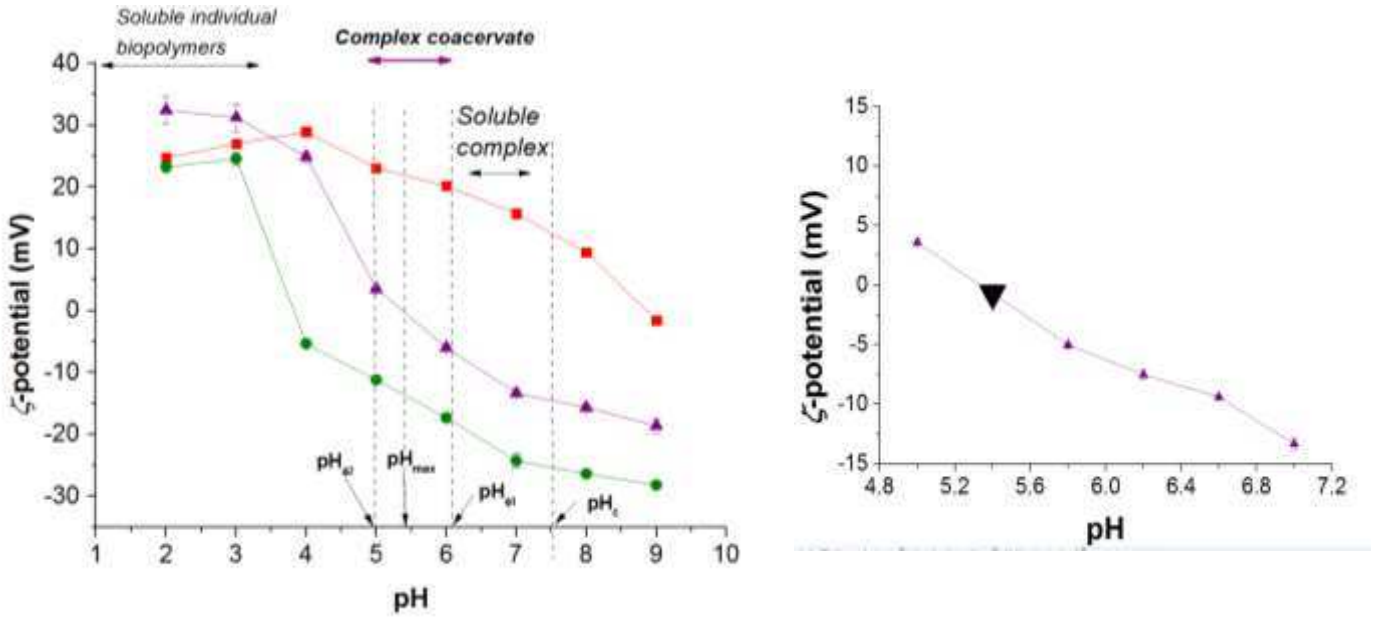

Figure 6. Mean ζ-potential values of 0.047 mM LF solution (■), 0.007 mM PPI solution (●) and mixture of 0.047 mM LF and 0.007 mM PPI solutions (▲) (PPI/ LF molar ratio of 0.15) as a function of pH showing pH_c, $pH_{\varphi 1}$, pH_{max}, and $pH_{\varphi 2}$ (A) and the zoomed-in mean ζ-potential values of LF-PPI mixtures in pH 5-7 region highlighting the isoelectric point (▼) (B). Error bars represent standard deviations.

346 Although the mechanism of the complex coacervate formation is not fully understood, we
347 hypothesize the following sequential processes based on previous literature. Below pH 4, both LF
348 and PPI molecules being cationic molecules (pH> pI) appear to repel each other and this prevents
349 the formation of a complex between the two protein molecules.

350 This is in line with the low particle size, turbidity measurements and transparent appearance
351 of the mixed biopolymer solutions (Figure 5). Dubin, et al. [28] showed that two polyelectrolytes that
352 contain like (negative or positive) charge could form soluble complex. Hence, in our case, the LF
353 and PPI might be present as individual biopolymer molecules or as soluble complexes below pH
354 4. Above pH 5.0, R_h gradually increased above the value that corresponds to the R_h of LF or PPI
355 alone observed for pH < $pH_{\phi 2}$ [25]. The pure (precipitate-free) coacervate formation appeared to be
356 initiated above pH 5.0, followed by growth of primary complexes to form quasi-neutralized
357 insoluble complexes ($pH_{\phi 2}$), with a depletion of charge at pH 5.0. Further kinetic experiments
358 should be performed to confirm this growth mechanism. At pH 5.4 (pH_{max}), electrical equivalence
359 was achieved between the proteins with ζ-potential reaching zero, the particle scattering being
360 highest with a steep rise in R_h (Figure 5B) and the turbidity reaching as well its maximum. This is
361 seen in other studies where LF has been shown to form coacervate with anionic proteins at this pH
362 range. For instance, Anema and de Kruif [14] observed maximum coacervation for β-lg (β-
363 lactoglobulin)-LF complexation at pH 6.3, where the ζ-potential was nearly zero. In our case,
364 coacervation is maximized at pH 5.4, which is closer to the pI of PPI than that of LF, as halfway
365 between the respective pI's would be pH 6.25 (=(4+8.5)/2).

366 Soluble complexes are formed between biopolymers when net charge is high and electrostatic
367 interaction is lower whereas insoluble complexes and coacervate formation occurs when
368 electrostatic interaction between molecules is strong and net charge was low. In our case, we

suggest that at pH 5.0-6.0 there was formation of coacervate, whereas ≥ $pH_{\phi 1}$ (6.2), soluble complexes were formed and the boundary is designated as pH_c (pH 7), i.e. 1.5 units away from isoelectric point of LF. Above pH 8.5, both LF and PPI carried a similar net charge. To reveal the distribution of size of these complexes and/or coacervates, small angle X-ray scattering (SAXS) and atomic force microscopy (AFM) were used.

3.4. Small Angle X-ray Scattering (SAXS).

The SAXS pattern of pure dispersions of LF and PPI were recorded at pH 7 at 25 °C and analyzed by the Generalized Indirect Fourier Transform (GIFT) method [29] (Figure 7). The determined SAXS data of LF and of PPI (Figure 7A) compared well to previous literature data [30-32]. As revealed in the PDDFs (Figure 7B) LF was not perfectly globular, but composed of two globular lobes, which are compactly arranged in protein crystals, but under solution conditions can open up. In solution, Grossmann et al. [31] determined a radius of gyration, R_g = 3.3-3.6 nm for human lactoferrin measured at pH 7.5. Since our samples were measured at a slightly lower pH, the difference in our observed value of R_g = 4.2 nm for bovine lactoferrin might be related to a bigger opening of the inter-domain cleft. Note, that the smallest cleft is observed in the crystal form of lactoferrin, in which the corresponding R_g is smaller than 3 nm [30, 31]. Concerning PPI, a maximum extension of about 25 nm and furthermore a double peak distribution is apparent in the PDDF. The PPI consisted mainly of legumin and vicilin and in minor part of convicilin (13%; referring to results from Fig. 2), and as discussed elsewhere [33]. We note, legumin has R_g = 4.45 nm [34] and vicilin has R_g = 4.4 nm [35].

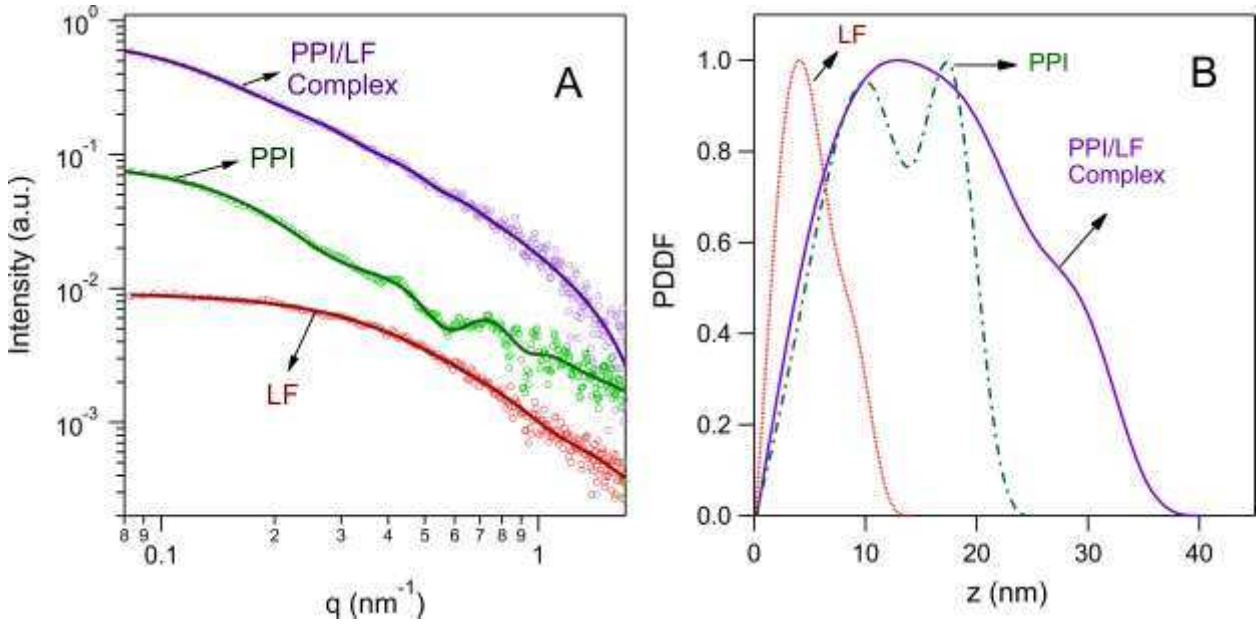

390

391 **Figure 7.** A) SAXS curves of 0.007 mM PPI, 0.047 mM LF and their complex formed at pH=7.
392 The solid lines represent the fitted curves obtained by Indirect Fourier Transformation (IFT)
393 analysis. B) The corresponding Pair-Distance Distribution Functions (PDDFs) are displayed as a
394 function of the radial distance (z).
395

396 Thus, the PDDF confirms that the PPI aggregates into oligomers (about 3-6 proteins), which was
397 first shown as a pseudo-hexagonal, ring-like appearance by scanning electron tunneling
398 microscopy [32]. The extension of PPI the ring-like aggregates is in the order of 20-25 nm, which
399 compares well to a maximum extension of about 25 nm displayed in the PDDF (Figure 7B).

400

401 **Table 1**. Radius of gyration of PPI, LF and their complex at pH 7.0.
402

Sample	Radius of gyration (nm)
LF	4.22
PPI	9.47
LF-PPI complex	13.1

403

404 Figure 8 gives an overview of all measured LF-PPI complexes and coacervates at various pH
405 values. As clearly shown at pH 7.0, complexes were composed of both LF and PPI, since a simple
406 superposition of the individual LF and PPI scattering curves would not lead to a SAXS curve with
407 R_g = 13.1 nm. Therefore, in this case the amount of self-aggregated protein can practically be
408 ignored. In accordance with the ζ-potential measurements (compare Figure 6), the biggest
409 coacervates were formed at pH 5.4. Their maximum extension reached values of about 80 nm
410 (Figure 8B), leading to rough estimate of coacervate radius of 40 nm. Since the majority of the
411 involved proteins (legumin and vicilin) have similar radii (R_g = 4.0 to 4.5 nm, which relates to R
412 = $\sqrt{\frac{5}{3}}\,R_g$ = 5.2 to 5.8 ≈ 5.5 nm), we can roughly estimate the number of proteins involved in the
413 biggest coacervates: $V_{coacervate}$ /$V_{protein}$ ≈ 380 proteins. Assuming a protein packing density similar
414 to the closest packing density of spheres (0.74), we obtain a corrected estimate of about 280
415 proteins per coacervate at pH 5.4. The highest solubility of proteins was determined for pH 6.2
416 (smallest R_g = 7.7 nm), which corresponds to about 4-5 proteins per complex. Further increasing
417 the pH increased the size of the complexes again: at pH 7, roughly 36 proteins were involved. We
418 note, however, that these are only indicative estimates, and should be taken with due care, as we
419 are considering ideal hard sphere packing of the proteins and also have not taking into account the

convicilin proteins. Importantly, a closer inspection of the PDDF's in Figure 8B reveals that the size distributions of the coacervates were not fully symmetric (note, that each PDDF displays a shoulder at higher distances). This bimodal size distribution was further confirmed by AFM measurements (see section 3.5) and can be assigned to differently shaped coacervates, *i.e.* to spherical and elliptically shaped complexes, respectively [36].

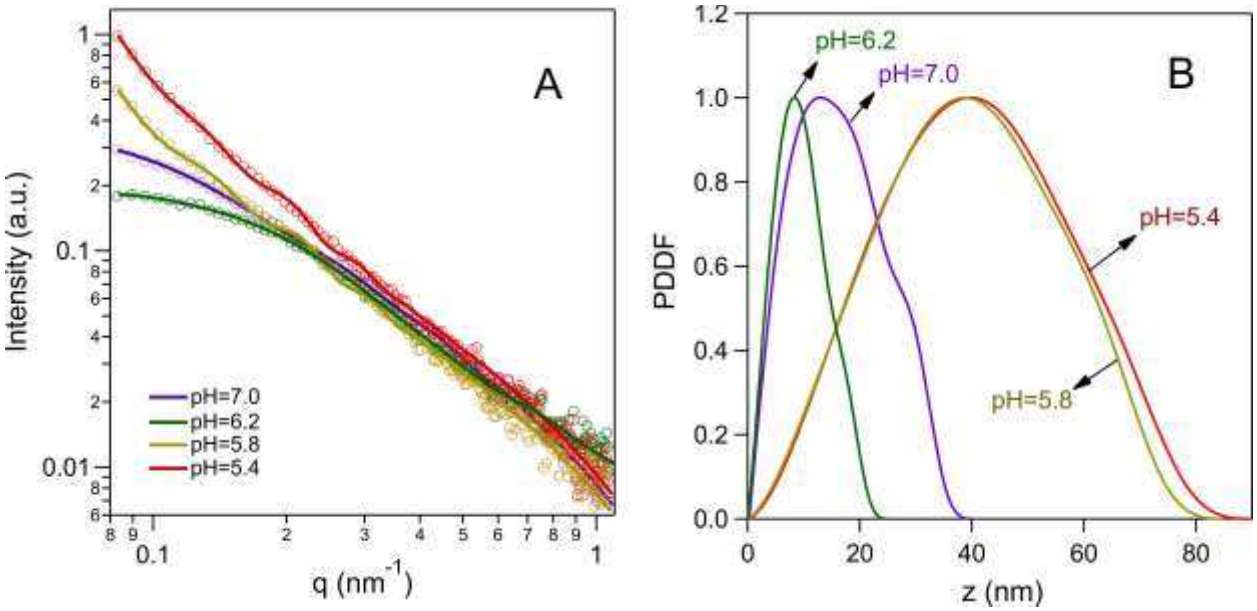

Figure 8. A) Small angle scattering curves of the LF-PPI coacervates and/or soluble complexes at various pH values. B) The corresponding Pair-Distance Distribution Functions (PDDFs) were evaluated based on Indirect-Fourier Transformation and show that the largest coacervate formed at pH=5.4.

Table 2. Radius of gyration of LF-PPI coacervates (at pH 5.4 and 5.8) and soluble complexes (at pH 6.2 and 7.0).

pH	Radius of Gyration (nm)
7.0	13.1
6.2	7.7
5.8	30.3
5.4	31.3

436 **3.5. AFM micrographs of the coacervates.**

437 Atomic force microscopy (AFM) images were analyzed to investigate structure of LF, LF-PPI
438 complex (pH 7.0) and LF-PPI coacervate (pH 5.4) adsorbed to mica surfaces (Figure 9). As can
439 be observed from Figure 9A and histogram a, LF showed uniform spherical particles, with a mean
440 radius of 6.2 nm. From SAXS, the lactoferrin radius was 4.2 nm. This increase in apparent size
441 can be described by the well-known tip-magnification effect in AFM. A tip radius of 7.5 nm,
442 typical of the TESPA-V2 (Bruker) probes used in this study, would result in an apparent size of
443 6.2 nm for the lactoferrin. The complexes formed at pH 7.0 were very sparse owing to a weak
444 electrostatic attachment, despite the use of the divalent cation Mg^{2+} to modify the surface of mica
445 [37]. This may be because of the influence of ionic strength change on the narrow boundary
446 conditions of LF-PPI complex and coacervate formation.

447 The radius of the soluble complexes (Figure 10Bb) from AFM images was found to lie in
448 the broader range between 9-15 nm (mean radius = 11.2 nm) which is in close agreement with
449 SAXS data (PPI: R_g = 9.5 nm, LF-PPI complex: R_g = 13.1 nm, both at pH 7.0). Most importantly,
450 the coacervates formed at pH 5.4 were clearly visible as groups of individual proteins forming
451 complexes of greater than 40 nm in size. The analysis of complex morphology is shown in Figure
452 10. While a dense and space filling structure of coacervates was formed at pH 5.4 (Figure 9C), the
453 complexes produced at pH 7.0 (Figure 9B) were less clustered. Figure 9D shows the detail of the
454 large single coacervate in topography and AFM phase contrast. Below, we present a schematic
455 representation created from circular unit with measurements taken from the AFM images of pure
456 LF and PPI and overlaid onto the image (Figure 9D top) as closely as possible. The underlying
457 image was then deleted to reveal a stylised cartoon of the coacervate, which suggests that LF were
458 forming bridges between predominantly PPI moieties forming the structural units. Bottom panel

459 is a cartoon illustration of the same complexes, made up of LF (red small circles) and PPI (blue
460 large circles) scaled using the mean individual protein size from the histograms.

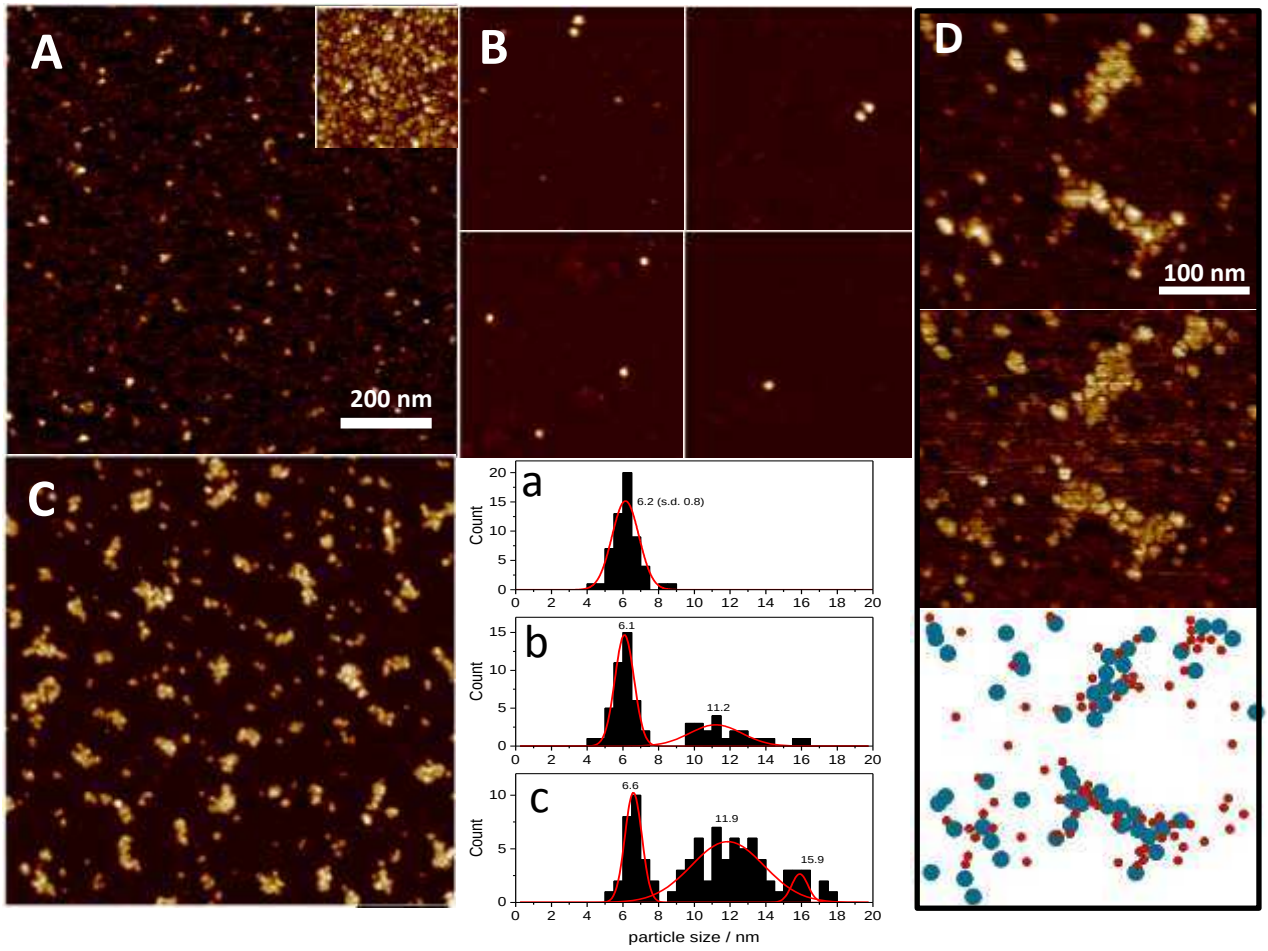

461

462 **Figure 9.** Tapping mode AFM images with size analysis histograms of individual proteins, either
463 as isolated particles or when they can be clearly discriminated within complexes. A-a LF at pH 7.0
464 (inset shows image of continuous close packed layer of LF prepared from a higher concentration
465 solution), B-b LF-PPI complex at pH 7.0 (the pH 7.0 complex did not bind well to mica and were
466 sparsely distributed, so shown here are a composite of 4 separate 500 nm scans), C-c LF-PPI
467 coacervate at pH 5.4. Histogram of diameters, a-c, is for entities < 20 nm radius only. Images A-
468 C are to the same scale. D Coacervates at pH 5.4 at higher resolution. Top panel is AFM
469 topography, middle panel is an AFM phase contrast image of the same area, which shows the
470 protein has a different material response to the background mica substrate (as expected) and the
471 sensitivity of the mode to gradient helps discriminate individual proteins.

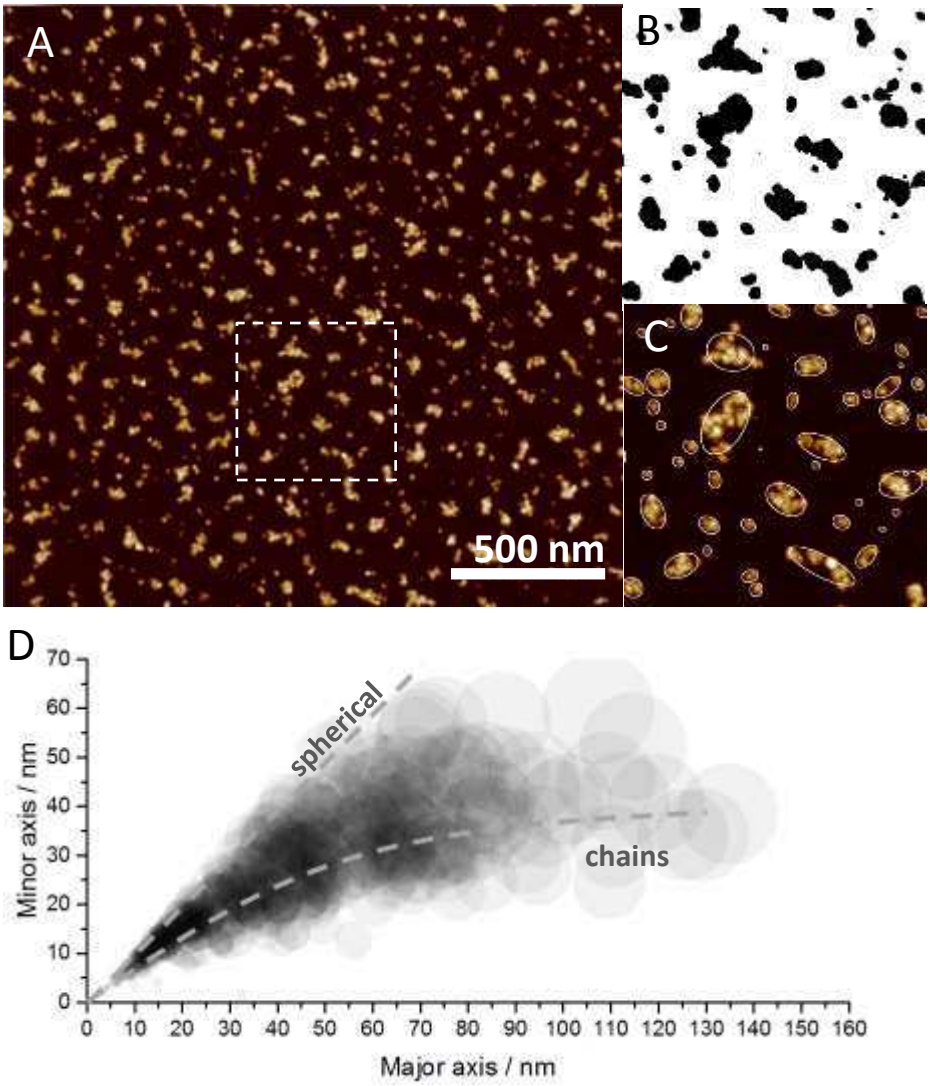

Figure 10. A) AFM topography image of pH 5.4 coacervate at 2048 pixel resolution, B**)** digital zoom of area highlighted in panel A, thresholded to create a binary image before automated particle analysis, C) software fits ellipses to each aggregate, shown here overlaid upon the digital zoom of the original image. The major and minor axis of each ellipse is used to generate panel D), describing the size and shape distribution of >1000 complexes. The size of each data point has been scaled to the size of the complex, hence the intensity reflects the probability of each protein particle to be aggregated within a complex of a particular size/shape. Complexes up to 140 nm in length were found, which tended to be limited to a width of around 40 nm.

The distribution of particle sizes is represented in Figure 10D, which shows the length and width of each particle. As there are many more individual particles of smaller size (40-80 nm range), and a fewer number of large aggregates containing much more of the total mass of coacervate, the size

of each data point was scaled to be directly proportional to the size of each particle. This better represents the most likely size and shape of the coacervate, and hence directly comparable to SAXS data. Overall, the distribution contained strong clusters of the axis lengths around 40-50 nm (minor axis) and 60-80 nm (major axis), which agrees well with the SAXS-derived PDDA data (Figure 8B). More spherical clusters are represented by the straight line with the major and minor axes of the same size, whilst the elongated complexes by the distribution along the x-axis, with no further increase in width. Interestingly, the complexes appeared to grow directionally forming ordered chains with width of 30-50 nm. In fact, once the clusters start to grow, they were more likely to elongate, which might be facilitated by PPI-PPI linkages. We speculate that additional PPI-PPI linked aggregation might be responsible for the formation of clearly chain-like aggregates. Indeed, in rarer cases, elongated aggregates with a major axis length up to 140 nm and minor axis of 40 nm were observed (Figure 10D).

However, importantly, most frequent cluster sizes group around 40-80 nm with spherical to elliptical shapes (axis aspect ratio ≤ 2), whereas elongated to chain-like structures appeared to be less frequent. The latter has also been confirmed the SAXS data (Fig. 8A), where the low q-value data at pH 5.4 and 5.8 (referring to big particle sizes) were exclusively fitted with particle sizes up to 80 nm. Further, the concentration of clusters with elliptical shapes with typical axis ratios of 80 to 40 nm dominated over the purely spherical nanocomplexes of 40 nm (Figure 10D). This bimodal size distribution was also reflected in the SAXS data (Figure 8D). In conclusion, we believe that this major population of spherical and elliptical nanocomplexes were responsible for the formation of coacervate, shown by the liquid behavior of the dense viscous phase at a macroscopic scale post centrifugation. Similar spherical to elliptic shaped clusters have also been reported in other

coacervate systems, such as in bovine serum albumin (BSA) and poly(dimethyldiallylammonium chloride) (PDADMAC)[38] and polyelectrolyte-mixed micelle.[39]

4. CONCLUSIONS

Mixing cationic lactoferrin (LF) and anionic pea protein isolate (PPI) lead to complex formation and coacervate formation under specific conditions of pH range with maximum level of coacervate formation observed at charge neutrality. The DLS, ζ-potential data and turbidity measurements enabled identification of the optimum pH conditions where coacervation was most favorable (pH 5.4), and where soluble complexes were maximized (pH 7). The SAXS measurements confirmed the formation of heteroprotein complexes with a radius of gyration of ~13 nm at pH 7. Coacervates with maximum extensions of about 80 nm were observed at pH 5.4. Both, the bimodal size distribution and characteristic length scales deduced from SAXS data are in excellent agreement with the AFM analysis, showing a distribution containing frequent clusters with particles sizes around 40-80 nm, with a predominance of elliptical over spherical LF-PPI coacervates. However, with respect to the rarer observed chain-like aggregations, additionally facilitated PPI-PPI aggregation cannot be fully ignored and thus the interplay between LF-PPI coacervation and PPI-PPI aggregation mediated clusters requires further investigation. Future studies are needed to understand the electrostatic interactions between LF and pure individual fractions of legumin, vicillin and convicilin from pea sources, respectively.

SUPPLEMENTARY INFORMATION

< Details of solubility curve of PPI stock solution, raw correlograms of LF and PPI stock solutions (DLS) and turbidity curves of LF-PPI mixtures as a function of pH are reported>

AUTHOR INFORMATION

Corresponding Author

*Email: A.Sarkar@leeds.ac.uk

Food Colloids and Processing Group,

School of Food Science and Nutrition, University of Leeds, Leeds, LS2 9JT, United Kingdom.

AUTHOR CONTRIBUTIONS

AnS initiated and designed the research, EA performed the experiments, SDC performed AFM, AmS performed SAXS. AnS, EA, SDC and MR analysed the data. The manuscript was written through contributions of all authors. AnS had primary responsibility for final content. All authors have given approval to the final version of the manuscript.

ACKNOWLEDGMENT

Author (EA) kindly acknowledges TUBITAK Visiting fellowship for conducting this research at University of Leeds as a part of her PhD studies.

REFERENCES

1. Salvatore, D.; Croguennec, T.; Bouhallab, S.; Forge, V.; Nicolai, T., Kinetics and structure during self-assembly of oppositely charged proteins in aqueous solution. Biomacromolecules **2011,** 12, (5), 1920-1926.

2. Hwang, D. S.; Zeng, H.; Srivastava, A.; Krogstad, D. V.; Tirrell, M.; Israelachvili, J. N.; Waite, J. H., Viscosity and interfacial properties in a mussel-inspired adhesive coacervate. Soft Matter **2010,** 6, (14), 3232-3236.

3. Toh, Y.-C.; Ho, S. T.; Zhou, Y.; Hutmacher, D. W.; Yu, H., Application of a polyelectrolyte complex coacervation method to improve seeding efficiency of bone marrow stromal cells in a 3D culture system. Biomaterials **2005,** 26, (19), 4149-4160.

4. Jin, K.-M.; Kim, Y.-H., Injectable, thermo-reversible and complex coacervate combination gels for protein drug delivery. J. Controlled Release **2008,** 127, (3), 249-256.

5. Bi-cheng, W.; Brian, D.; David Julian, M., Soft matter strategies for controlling food texture: formation of hydrogel particles by biopolymer complex coacervation. Journal of Physics: Condensed Matter **2014,** 26, (46), 464104.

6. Schmitt, C.; Sanchez, C.; Desobry-Banon, S.; Hardy, J., Structure and technofunctional properties of protein-polysaccharide complexes: A review. Critical Reviews in Food Science and Nutrition **1998,** 38, (8), 689-753.

7. Chapeau, A.-L.; Tavares, G. M.; Hamon, P.; Croguennec, T.; Poncelet, D.; Bouhallab, S., Spontaneous co-assembly of lactoferrin and β-lactoglobulin as a promising biocarrier for vitamin B9. Food Hydrocolloids **2016,** 57, 280-290.

8. Tavares, G. M.; Croguennec, T.; Hamon, P.; Carvalho, A. F.; Bouhallab, S., Selective coacervation between lactoferrin and the two isoforms of β-lactoglobulin. Food Hydrocolloids **2015,** 48, 238-247.

9. Yan, Y.; Kizilay, E.; Seeman, D.; Flanagan, S.; Dubin, P. L.; Bovetto, L.; Donato, L.; Schmitt, C., Heteroprotein complex coacervation: Bovine β-lactoglobulin and lactoferrin. Langmuir **2013,** 29, (50), 15614-15623.

10. Flanagan, S. E.; Malanowski, A. J.; Kizilay, E.; Seeman, D.; Dubin, P. L.; Donato-Capel, L.; Bovetto, L.; Schmitt, C., Complex equilibria, speciation, and heteroprotein coacervation of lactoferrin and β-lactoglobulin. Langmuir **2015,** 31, (5), 1776-1783.

11. Kizilay, E.; Seeman, D.; Yan, Y.; Du, X.; Dubin, P. L.; Donato-Capel, L.; Bovetto, L.; Schmitt, C., Structure of bovine β-lactoglobulin-lactoferrin coacervates. Soft Matter **2014,** 10, (37), 7262-7268.

12. Peixoto, P. D. S.; Tavares, G. M.; Croguennec, T.; Nicolas, A.; Hamon, P.; Roiland, C.; Bouhallab, S., Structure and dynamics of heteroprotein coacervates. Langmuir **2016,** 32, (31), 7821-7828.

582 13. Du, X.; Seeman, D.; Dubin, P. L.; Hoagland, D. A., Nonfreezing water structuration in
583 heteroprotein coacervates. Langmuir **2015,** 31, (31), 8661-8666.

584 14. Anema, S. G.; de Kruif, C. G., Phase separation and composition of coacervates of
585 lactoferrin and caseins. Food Hydrocolloids **2016,** 52, 670-677.

586 15. Anema, S. G.; de Kruif, C. G., Interaction of lactoferrin and lysozyme with casein
587 micelles. Biomacromolecules **2011,** 12, (11), 3970-3976.

588 16. Anema, S. G.; de Kruif, C. G., Complex coacervates of lactotransferrin and beta-
589 lactoglobulin. J. Colloid Interface Sci. **2014,** 430, 214-220.

590 17. Nigen, M.; Croguennec, T.; Madec, M.-N.; Bouhallab, S., Apo α-lactalbumin and
591 lysozyme are colocalized in their subsequently formed spherical supramolecular assembly. FEBS
592 J. **2007,** 274, (23), 6085-6093.

593 18. Nigen, M.; Croguennec, T.; Renard, D.; Bouhallab, S., Temperature affects the
594 supramolecular structures resulting from α-lactalbumin−lysozyme interaction. Biochemistry
595 **2007,** 46, (5), 1248-1255.

596 19. AOAC, Official methods of analysis of Association of Official Analytical Chemists In
597 Washington, DC, USA, 1995.

598 20. Patil-Sen, Y.; Sadeghpour, A.; Rappolt, M.; Kulkarni, C. V., Facile preparation of
599 internally self-assembled lipid particles stabilized by carbon nanotubes. J. Visualized Exp. **2016**,
600 (108), e53489.

601 21. Barac, M.; Cabrilo, S.; Pesic, M.; Stanojevic, S.; Zilic, S.; Macej, O.; Ristic, N., Profile
602 and functional properties of seed proteins from six pea (Pisum sativum) genotypes. Int. J. Mol.
603 Sci. **2010,** 11, (12), 4973-4990.

604 22. Mertens, C.; Dehon, L.; Bourgeois, A.; Verhaeghe-Cartrysse, C.; Blecker, C.,
605 Agronomical factors influencing the legumin/vicilin ratio in pea (Pisum sativum L.) seeds. J. Sci.
606 Food Agric. **2012,** 92, (8), 1591-1596.

607 23. Liu, S.; Low, N. H.; Nickerson, M. T., Effect of pH, salt, and biopolymer ratio on the
608 formation of pea protein isolate−gum arabic complexes. J. Agric. Food Chem. **2009,** 57, (4),
609 1521-1526.

610 24. Qazvini, N. T.; Bolisetty, S.; Adamcik, J.; Mezzenga, R., Self-healing fish gelatin/sodium
611 montmorillonite biohybrid coacervates: Structural and rheological characterization.
612 Biomacromolecules **2012,** 13, (7), 2136-2147.

613 25. Kizilay, E.; Kayitmazer, A. B.; Dubin, P. L., Complexation and coacervation of
614 polyelectrolytes with oppositely charged colloids. Adv. Colloid Interface Sci. **2011,** 167, (1–2),
615 24-37.

26. Gharsallaoui, A.; Cases, E.; Chambin, O.; Saurel, R., Interfacial and emulsifying characteristics of acid-treated pea protein. Food Biophys **2009,** 4, (4), 273-280.

27. Croguennec, T.; Tavares, G. M.; Bouhallab, S., Heteroprotein complex coacervation: A generic process. Adv. Colloid Interface Sci. **Accepted, In Press** (10.1016/j.cis.2016.06.009).

28. Dubin, P. L.; Gao, J.; Mattison, K., Protein-Purification by Selective Phase-Separation with Polyelectrolytes. Sep. Purif. Methods **1994,** 23, (1), 1-16.

29. Bergmann, A.; Fritz, G.; Glatter, O., Solving the generalized indirect Fourier transformation (GIFT) by Boltzmann simplex simulated annealing (BSSA). J. Appl. Crystallogr. **2000,** 33, (5), 1212-1216.

30. Anderson, B. F.; Baker, H. M.; Dodson, E. J.; Norris, G. E.; Rumball, S. V.; Waters, J. M.; Baker, E. N., Structure of human lactoferrin at 3.2-A resolution. Proc. Natl. Acad. Sci. U. S. A. **1987,** 84, (7), 1769-1773.

31. Grossmann, J. G.; Neu, M.; Pantos, E.; Schwab, F. J.; Evans, R. W.; Townes-Andrews, E.; Lindley, P. F.; Appel, H.; Thies, W.-G.; Hasnain, S. S., X-ray solution scattering reveals conformational changes upon iron uptake in lactoferrin, serum and ovo-transferrins. J. Mol. Biol. **1992,** 225, (3), 811-819.

32. Welland, M. E.; Miles, M. J.; Lambert, N.; Morris, V. J.; Coombs, J. H.; Pethica, J. B., Structure of the globular protein vicilin revealed by scanning tunnelling microscopy. Int. J. Biol. Macromol. **1989,** 11, (1), 29-32.

33. Mession, J.-L.; Sok, N.; Assifaoui, A.; Saurel, R., Thermal denaturation of pea globulins (Pisum sativum L.)—Molecular interactions leading to heat-induced protein aggregation. J. Agric. Food Chem. **2013,** 61, (6), 1196-1204.

34. Plietz, P.; Zirwer, D.; Schlesier, B.; Gast, K.; Damaschun, G., Shape, symmetry, hydration and secondary structure of the legumin from Vicia faba in solution. Biochim. Biophys. Acta, Protein Struct. Mol. Enzymol. **1984,** 784, (2), 140-146.

35. I'Anson, K. J.; Miles, M. J.; Bacon, J. R.; Carr, H. J.; Lambert, N.; Morris, V. J.; Wright, D. J., Structure of the 7S globulin (vicilin) from pea (Pisum sativum). Int. J. Biol. Macromol. **1988,** 10, (5), 311-317.

36. Dmitri, I. S.; Michel, H. J. K., Small-angle scattering studies of biological macromolecules in solution. Rep. Prog. Phys. **2003,** 66, (10), 1735.

37. Pastré, D.; Piétrement, O.; Fusil, S.; Landousy, F.; Jeusset, J.; David, M.-O.; Hamon, L.; Le Cam, E.; Zozime, A., Adsorption of DNA to mica mediated by divalent counterions: A theoretical and experimental study. Biophys. J. **2003,** 85, (4), 2507-2518.

38. Kaibara, K.; Okazaki, T.; Bohidar, H. B.; Dubin, P. L., pH-Induced coacervation in complexes of bovine serum albumin and cationic polyelectrolytes. Biomacromolecules **2000,** 1, (1), 100-107.

39. Liberatore, M. W.; Wyatt, N. B.; Henry, M.; Dubin, P. L.; Foun, E., Shear-induced phase separation in polyelectrolyte/mixed micelle coacervates. Langmuir **2009,** 25, (23), 13376-13383.

656 **TABLE OF CONTENTS (GRAPHIC)**

657

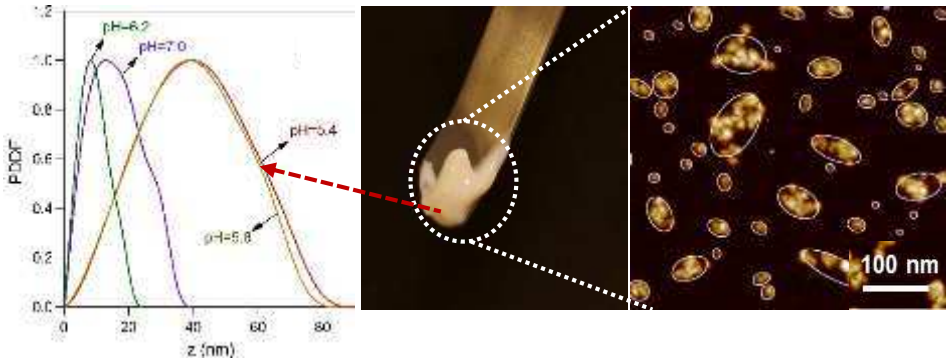

658